metals

MDPI

Article

The Anisotropic Stress-Induced Diffusion and Trapping of Nitrogen in Austenitic Stainless Steel during Nitriding

Arvaidas Galdikas * and Teresa Moskalioviene

Physics Department, Kaunas University of Technology, Studentu 50, LT-51368 Kaunas, Lithuania; mgmf.fk@ktu.lt

* Correspondence: arvaidas.galdikas@ktu.lt; Tel.: +370-600-48897

Received: 3 August 2020; Accepted: 30 September 2020; Published: 1 October 2020

Abstract: Plasma nitriding of austenitic stainless steels at moderate temperatures is considered in the presented work. The anisotropic aspects of stress-induced diffusion and influence of nitrogen traps are investigated by kinetic modeling based on rate equations. The model involves diffusion of nitrogen in the presence of internal stress gradients induced by penetrating nitrogen as the next driving force of diffusion after the concentration gradient. The diffusion equation takes into account the fact that nitrogen atoms reside in interstitial sites and in trapping sites. Stress-induced diffusion has an anisotropic nature and depends on the crystalline orientation while trapping–detrapping is isotropic. The simulations are done considering the synergetic effects of both mechanisms and analyzing the properties of both processes separately. Theoretical curves are compared with experimental results taken from the literature. Good agreement between simulated and experimental results is observed, and gives the possibility to find real values of parameters needed for calculations. The nitrogen depth profile shapes, the dependences of nitrogen penetration on nitriding time and on diffusivity, are analyzed considering crystalline orientation of steel single crystal.

Keywords: austenitic stainless steel; plasma nitriding; stress-induced diffusion; trapping; kinetic modeling

1. Introduction

Plasma nitriding of austenitic stainless steel (ASS) at temperatures less than the formation of nitrides greatly increases surface hardness, corrosion, and wear resistance [1–13]. The nitriding creates lattice distortion of the FCC austenitic phase (γ phase), leading to the formation of nitrogen-rich expanded austenite (γ_N phase) [6,14]. The high nitrogen content dissolved in the γ_N crystalline lattice leads to a noticeable expansion and in some cases rotation [15] of the lattice, giving rise to high residual compressive stresses [9–12]. Intensive studies on γ_N phase structure and formation have been undertaken by various researchers in recent decades and a comprehensive review of the scientific literature regarding the formation, characteristics, and properties of the γ_N phase was presented in [16].

Many experiments show that the thickness of expanded austenite phase as well as nitrogen penetration depth depend on the crystal orientation and increase in the order (111) < (110) < (100) for different orientations [6,8,17–20]. The same order of crystalline orientations follows the nitrogen concentration on the surface. The difference of the thickness of expanded austenite phase was explained by lattice stress anisotropy, which gave rise to an orientation dependence of the activation energy for diffusion [21]. The effect of anisotropic lattice expansion could be explained by the residual

compressive stress developed during nitriding which varies as a function of crystalline orientation of the ASS specimen due to the elastically anisotropic nature of austenite [11,22,23]. The elastic field creates an additional driving force for the nitrogen transport [24–31]. Because of the elastic anisotropy of ASS, the induced internal stresses are dependent on the crystalline orientation and influence of nitrogen penetration depth, which becomes dependent on the crystalline orientation [31].

The content of nitrogen that penetrates into the bulk of the sample is influenced not only by the volumetric processes, but also by processes on the surface. Adsorption, desorption, and heterogeneous chemical reactions on the surface are very important processes during plasma nitriding. Adsorption and dissociation of molecules on the surface taking place during heterogeneous reactions depend on surface free energy [32]. Surface free energy depends on the orientation of the surface [32] which means that processes on the surface also have an anisotropic nature and influence the anisotropic nature of nitrogen penetration in the volume of austenite. The nitrogen fluxes passing through the surface of different crystalline orientations can be different due to the anisotropic nature of adsorption and heterogeneous chemical reactions on the surface [31].

Expanded austenite, which will be called γ_N phase in this paper, is known as a supersaturated solid solution of nitrogen in stainless steel with a disordered FCC structure and a distorted lattice [33]. It was shown the existence of short range ordering of Cr and N atoms takes place [33,34]. High content of nitrogen penetrating the volume of austenite has been attributed to the trapping of nitrogen at octahedral interstitial sites, by alloying element atoms dissolved in the matrix with high affinity for N such as Cr [18,34]. The role of Cr has been investigated to have pointed to ''trapping and detrapping'' diffusion of nitrogen [35]. In the trapping–detrapping model, chromium atoms play a crucial role via a chemical bonding effect where Cr atoms form trap sites for N [36]. The preferential bonding of chromium with nitrogen in the γ_N phase has been observed in AISI 304L with a ratio N/Cr very close to 1 [37], which supports the specific role of chromium in the atomic transport of nitrogen. The depth profiles calculated with the trapping–detrapping model are in excellent agreement with the experimental ones [17,38,39]. However, recently it was shown for "chromium-free" austenitic iron-nickel alloy that Cr is not a necessity for the nitrogen-interstitial-induced lattice expansion phenomenon to occur [35]. The penetration of nitrogen without assistance of chromium and the driving force is internal stresses which create stress-induced diffusion [24–30]. Moreover, a concentration-dependent diffusivity model has also been used to describe the behavior of nitrogen in stainless steel. The diffusivity of interstitial atoms in the γ_N phase seems to be dependent on their concentration. For example, Mandl et al. [40] calculated the nitrogen diffusivity from concentration profiles of N-implanted samples and they found that nitrogen diffusivity depends on concentration, with a high value for high nitrogen content and low value for low concentration. It has been hypothesized that the increase of the lattice constant during γ_N phase formation changes the electron density distribution, so that an increase of diffusivity occurs due to the lowered potential barriers between two interstitial sites. This model is also able to explain the carbon diffusivity in austenite [41]. In fact, many efforts have been made to explain this enhanced nitrogen diffusion, and several models have been suggested to correctly take into account the different phenomena which can influence it, and thus reproduce the experimental profiles.

Generally, the trapping of interstitial components such as hydrogen, carbon, or nitrogen at interstitial positions by different sorts of traps can be observed in metal alloys [42–46]. Nitrogen (or H and C) atoms move through a metal alloy by normal interstitial site diffusion or dislocation transport. The first description of this kind of trapping by Oriani [47] in 1970 can be considered to be a seminal contribution. Details on the application of Oriani relationships can be taken from the overviews [48–50]. Oriani's theory is based on considering a lattice consisting of two kinds of sites for occupancy by interstitial atoms. He postulates that the vast majority of sites are normal interstitial sites (NIS). The minor fraction of sites called trapping sites (TS) provides an energetically favorable environment for occupancy by the interstitial atoms. In ASS, chromium atoms play a crucial role via a chemical bonding effect where Cr atoms form trap sites for nitrogen. Consequently, here we consider ASS lattice consisting of two kinds of sites for occupancy by nitrogen, i.e., diffusion sites where nitrogen can diffuse and trap sites (Cr atoms) where nitrogen cannot diffuse.

The attempt to combine both effects, stress-induced diffusion and trapping–detrapping was made in [24,25], where the effects of plasticity and dependence of diffusion coefficient on concentration, and inverse modeling of the surface reaction rate were also included. In this work we present combined modeling including stress-induced diffusion and trapping–detrapping process, taking into account and focusing on the anisotropy of internal stresses with respect to crystalline orientation and anisotropy of adsorption process on the surface of the ASS. The modeling relates to single crystals of stainless steels and is not directly applicable to polycrystals, where lateral diffusion fluxes, grain-to-grain mechanical interaction, and different surface conditions play a role.

2. Mass Transport Model—The Coupling Between Nitrogen Stress-Assisted Diffusion and Trapping

The diffusive flux of the interstitial atoms (J_N) contributes to the change in nitrogen concentration both in the lattice, C_{Ndif}, and in the traps, C_{Ntrap}. Therefore, based on Fick's second law the interstitial atoms diffusion through the austenite phase can be written as [36,38,39,46]:

$$\frac{\partial C_{Nsum}}{\partial t} = \frac{\partial}{\partial t}\left(C_{Ndif} + C_{Ntrap}\right) = -\nabla \cdot J_N \tag{1}$$

Generally, the main driving force for interstitial atom diffusion in the metallic lattice is the chemical potential gradient which depends on the nitrogen concentration field, and on the stress field. The interstitial nitrogen causes an expansion of the crystal lattice of the austenite phase. This phenomenon implies the occurrence of local stresses, induced by nitrogen concentration gradients, and influences nitrogen transport in the expanded austenite phase. A systematic model for nitrogen transport in ASS that takes into account nitrogen diffusion and stress interaction was proposed in our previous works [26–31]. A generalized chemical potential and a diffusive flux are addressed to the freely diffusing nitrogen and according the stress-assisted diffusion model, the relationship between them attains the following form

$$J_N = -D\nabla C_{Ndif} + \frac{D \cdot C_{Ndif} \cdot V_N}{k_B \cdot N_A \cdot T}\nabla\sigma \tag{2}$$

where D is the diffusion coefficient of interstitial atoms in a stress-free solid, σ is the hydrostatic stress, V_N is the partial molar volume of interstitial in the solid matrix; T is the absolute temperature; k_B and N_A are Boltzmann constant and Avogadro constant, respectively.
Inserting Equation (2) into Equation (1) yields

$$\frac{\partial C_{Ndif}}{\partial t} + \frac{\partial C_{Ntrap}}{\partial t} = \nabla\left(D\nabla C_{Ndif}\right) + \nabla\left(\frac{D \cdot V_N \cdot C_{Ndif}}{k_B \cdot N_A \cdot T}\nabla\sigma\right) \tag{3}$$

In Equation (3) there are two unknowns C_{Ndif} and C_{Ntrap}. However following Oriani's theory the nitrogen concentration in the lattice was assumed to be in equilibrium with the concentration in the traps. This means that once the concentration in the lattice is known, we can calculate the concentration in the traps [39,46,47]:

$$\frac{\partial C_{Ntrap}}{\partial t} = K \cdot \left[C_{NDif}(H_t - C_{Ntrap}) - N_0 \cdot C_{Ntrap} \cdot \exp\left(\frac{-E_B}{k_B T}\right)\right] \tag{4}$$

where $K = 4\pi R_t \cdot D$; $D = D_0 e^{-E_A/k_B T}$; H_t is concentration of traps; N_0 is the concentration of host atoms; E_A is the diffusion activation energy; D_0 is the pre-exponential factor of diffusion; E_B is the detrapping activation energy; R_t is a characteristic capture radius of an individual trap site taken as the lattice constant; k_B is Boltzmann constant.

To evaluate the compressive stress and the compositional strain induced by the interstitial atom diffusion in the expanded austenite, a mechanical model recently proposed in our previous work [29,31] was used. This model is based on the Hooke's law and considers elastic anisotropy of ASS.

The dependence of compositionally induced biaxial compressive residual stresses in the [*hkl*] direction on concentration of interstitials can be determined by [29,31,50,51]:

$$\sigma(hkl) = \frac{1}{\left(S_{11} - P_{hkl} \cdot S_{44}(Z-1)\right)} \cdot \frac{\beta_N}{a_0} \cdot C_{Nsum} = -X_{stress(hkl)} \cdot C_{Nsum} \quad (5)$$

The anisotropic stress factor $X_{stress(hkl)}$ in any crystallographic direction [*hkl*] depends on so-called orientation factor $P_{hkl} = \left(h^2 \cdot k^2 + h^2 \cdot l^2 + k^2 \cdot l^2\right) \cdot \left(h^2 + k^2 + l^2\right)^{-2}$ [50] and on the Young's modulus $E_{hkl} = \left(S_{11} - 2 \cdot P_{hkl} \cdot \left(S_{11} - S_{12} - \frac{1}{2}S_{44}\right)\right)^{-1} = \left(S_{11} - P_{hkl} \cdot S_{44}(Z-1)\right)^{-1}$, where *h*, *k*, *l* are Miller indexes, S_{11}, S_{12}, S_{44} are independent intrinsic single crystal elastic constants (elastic compliances) and Zener ratio [52] $Z = \frac{2\left(S_{11} - S_{12}\right)}{S_{44}}$, which is perhaps the best known measure of the anisotropy of elastic behavior for crystals with cubic symmetry. In addition, a linear relation exists between the total strain in the [*hkl*] direction (which is linearly related to the stress through Hooke's law, i.e., $\varepsilon(hkl) = \frac{1}{E_{hkl}} \cdot \sigma(hkl)$) and the mean concentration of interstitials in the expanded austenite, i.e., $\varepsilon(hkl) = \frac{\beta_N}{a_0} \cdot C_{Nsum}$ [29], where β_N is the Vegard's constant for interstitial atoms dissolved in austenite and a_0 is the lattice parameter of the austenite (strain-free).

Introducing Equation (4) and Equation (5) into Equation (3) as the diffusion is one-dimensional along *x*-direction (1D diffusion problem, where *x*-axis is the diffusion axis), the mass transport of the nitrogen considering the effects of stress-assisted anisotropic diffusion and including the effects of traps is described by the following set of equations:

$$\frac{\partial C_{Ndif}}{\partial t} = \Phi_{0(hkl)} + \nabla x\left(D \nabla x C_{Ndif}\right) - \nabla x\left(\frac{D \cdot V_N \cdot C_{Ndif} \cdot X_{stress(hkl)}}{k_B \cdot N_A \cdot T} \nabla x C_{Nsum}\right) - \frac{\partial C_{Ntrap}}{\partial t} \quad (6)$$

$$\frac{\partial C_{Ntrap}}{\partial t} = K \cdot \left[C_{NDif}\left(H_t - C_{Ntrap}\right) - N_0 \cdot C_{Ntrap} \cdot \exp\left(\frac{-E_B}{k_B T}\right)\right] \quad (7)$$

$$\frac{\partial C_{Nsum}}{\partial t} = \frac{\partial C_{Ndif}}{\partial t} + \frac{\partial C_{Ntrap}}{\partial t} \quad (8)$$

where ∇_x is *x*-axis projection of gradient and $\Phi_{0(hkl)}$ is the anisotropic adsorption term, which describes the process of interstitial atom adsorption on the steel surface (i.e., for $x = 0$): $\Phi_{0(hkl)} = i_N \cdot \alpha_{N(hkl)} \cdot \left(N_0 - C_{Ndif}(0,t) - C_{Ntrap}(0,t)\right)$, where i_N—the relative flux of incident nitrogen atoms to the surface; $\alpha_{N(hkl)} = \alpha_N \cdot \left(h^2 + k^2 + l^2\right)^{-1/2}$—the crystal orientation dependent nitrogen adsorption probability [29,31].

3. Results and Discussion

In Figure 1, the fitting results of experimentally measured nitrogen depth profiles by proposed model are presented. Experimental results are taken from [19]. In those experiments the 316L ASS bulk single crystals with [100], [110], and [111] crystalline orientations have been plasma-nitrided for 1.00 h at either 573 or 673 K. The specimens were nitrided in the plasma reactor [53] where plasma is created by a 13.56 MHz electromagnetic excitation with an incident input power of 700 W. The gas mixture and the total pressure were 60% N_2 + 40% H_2 and 7.5 Pa, respectively. Treatments were performed under floating potential conditions. Detailed description of the sample preparation and

plasma conditions are reported in [19,53]. Nitrogen depth profiles were determined by method of nuclear reaction analysis (NRA). The values of parameters used for calculations are collected in Table 1. Theoretical curves 1.1–1.3 very well correspond with experimental points for all three different crystalline orientations. Comparison of the theoretical predictions with experimental data was considered good if the relative deviations of the calculated values from the experimental values was in the range from 0 to 5 % everywhere. The characteristic plateau, which typical for nitrogen distribution in plasma-nitrided ASSs, is well expressed. Previously, in [38] it was made attempt to fit theses experimental points by second Fick's law, assuming crystalline orientation dependent diffusion coefficient. In our calculations, we alternatively show that by taking into account anisotropy of crystal lattice stress-induced diffusion, the good fitting can be obtained with constant diffusion coefficient. Results presented in Figure 1 are calculated with the same diffusion coefficient for all different lattice orientation of single crystals, but with different parameter X_{stress} and different adsorption coefficient $\alpha_{N\text{-}hkl}$. The anisotropy of adsorption was discussed in our previous work [29,31]. By this we show that anisotropy of lattice stresses is mainly responsible for anisotropy of nitrogen penetration. However, the anisotropy of diffusion coefficient itself also cannot be neglected, because of lattice orientation dependence of the diffusion activation energy [21].

Table 1. Simulation parameters.

Elastic constants	AISI 316L γ Phase [54]	AISI 316L γ_N Phase [55]	T, K	673,573
			i_N, s^{-1}	27.2×10^{-4}
C_{11}, GPa	206	307.2	D_0, m^2s^{-1}	17.5×10^{-9}
C_{12}, GPa	133	134.1	E_A, eV [39]	1.1
C_{44}, GPa	119	46	E_B, eV	0.23
			α_N	0.8
$S_{11} = \frac{(C_{11}+C_{12})}{(C_{11}-C_{12})(C_{11}+2C_{12})}$, 1/GPa	0.00984	0.00443	$\alpha_{N\text{-}hkl}$	$\alpha_N \cdot \left(h^2+k^2+l^2\right)^{-1/2}$
$S_{12} = \frac{-C_{12}}{(C_{11}-C_{12})(C_{11}+2C_{12})}$, 1/GPa	−0.00386	−0.00135	X_{stress}, GPa presented in Figure 2	$\frac{\beta_N}{\left(S_{11}-P_{hkl}\cdot S_{44}(Z-1)\right)\cdot a_0}$
$S_{44} = \frac{1}{C_{44}}$, 1/GPa	0.00840	0.02174	N_0, m^{-3} [39]	7.29×10^{28}
			H_t, m^{-3} [39]	1.31×10^{28}
Zener ratio $Z = \frac{2(S_{11}-S_{12})}{S_{44}}$	3.26	0.53	V_N, m^3/mol	3.9×10^{-5}
			R_t, m [39]	0.38×10^{-9}

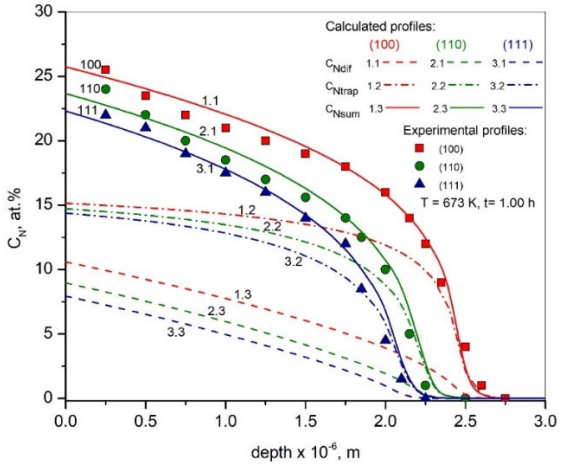

Figure 1. Calculated (lines) and experimental (points) (data from [19]) depth profiles of nitrogen: solid lines 1.1–3.1 resulting nitrogen profiles in the (100), (110) and (111) oriented single crystals of ASS, dotted lines 1.2–3.2 nitrogen in trap sites and dotted lines 1.3–3.3 diffusing nitrogen. Nitriding temperature 673 K.

In model Equations (6)–(8) there are two types of nitrogen: nitrogen in trap sites C_{Ntrap} and diffusing (free) nitrogen C_{Ndif}. In Figure 1 the depth distributions of both types of nitrogen are shown by dotted lines. These curves show that the plateau in nitrogen depth profile is formed mainly because of nitrogen distribution in traps sites, which is related with distribution of chromium. The plateau in curves 1.2–3.2 (nitrogen in trap sites) is very well expressed. The profiles of diffusing nitrogen, curves 1.3–3.3, also differ from Fickian depth profiles, because of inclusion of stress-induced diffusion. A not well expressed but observable plateau also can be observed in those curves. In general, the trapping–detrapping process is isotropic. However, as can be seen in Figure 1, the dependence on crystalline orientation is seen for profiles of trapped nitrogen (curves 1.2–3.2). That occurs because of anisotropy of stress-induced diffusion, higher diffusion, and more nitrogen arises which can be trapped in trap sites. As a result, more nitrogen in trap sites is for those crystalline orientation crystals for which diffusion is faster. In Figure 1 (curves 1.2–3.2), it can be seen that near the surface, where almost all trap sites are occupied by nitrogen atoms, the dependence on crystalline orientation of the amount of nitrogen in trap sites is much less expressed.

A very important parameter, which defines the anisotropic character of nitrogen depth profiles, is X_{stress}, which as shown above, is the function of Miller indexes and elastic compliances S_{ij}. Elastic compliances depend on phase of material. As discussed above, during nitriding of ASS AISI 316L the phase changes from austenite γ phase to expanded austenite γ_N phase. The elastic compliances change as well, and their change together changes the parameter X_{stress}. The parameter X_{stress} for each three considered crystalline orientations was calculated using values of elastic coefficients C_{ij} (which are related with elastic compliances S_{ij} (see Table 1)) taken form [54] and [55] for γ and γ_N phases, correspondingly. During kinetic modeling, when concentration of nitrogen rises from zero, it is important to consider the transition period, until γ_N phase is fully formed. It is known that expanded austenite phase forms at about 5 at.% of nitrogen [40]. In the interval 0 at.% < $C_N \leq$ 5 at.% of nitrogen concentration the transition period takes place. For the transition period we assume that parameter X_{stress} depends on nitrogen concentration and exponentially passes from values for γ phase to values for γ_N phase. The transition functions and dependences of parameter X_{stress} for each lattice orientation are shown in Figure 2. Please note that values of X_{stress} for γ_N phase decreases in order as (100) > (110) > (111) while for γ it occurs in opposite. That is just the result of elastic coefficient C_{11} which significantly increases and coefficients C_{44} which significantly decreases going from γ phase to γ_N phase. (see Table 1).

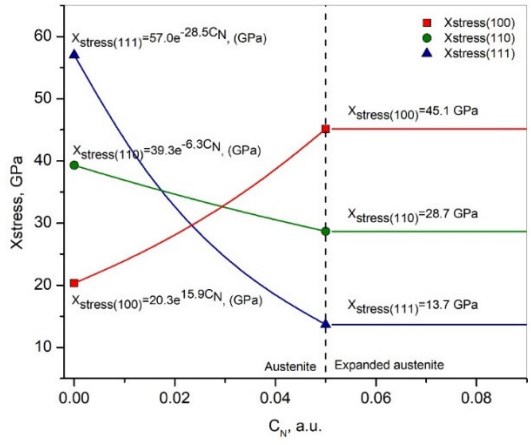

Figure 2. The transition functions and dependences of anisotropic stress factor X_{stress} on nitrogen concentration in the transition period from austenite phase γ to expanded austenite phase γ_N for each crystalline orientation.

The model presented in this work involves two processes, trapping–detrapping (TD) and lattice stress induce diffusion (SID). It is interesting to consider the properties of each of them. In Figure 3

there are presented calculated results for three cases: (1) including both processes TD and SID (curves 1.1–1.3), (2) only one process SID (curves 2.1–2.3) and (3) including only TD model (curves 3.1–3.3). All parameters for calculation are used the same as for curve (100) in Figure 1 (see Table 1).

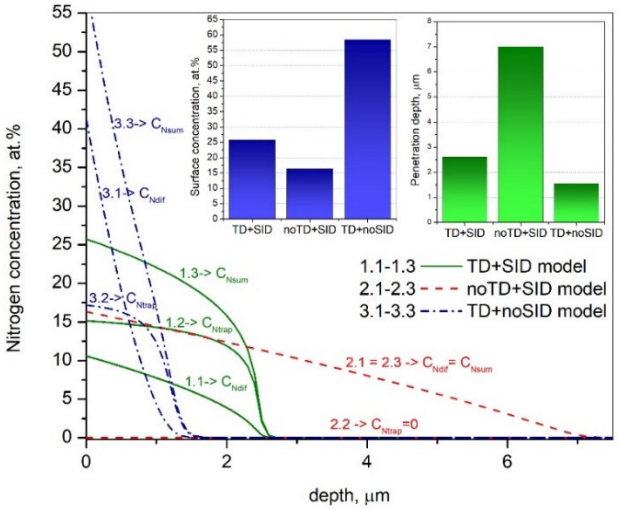

Figure 3. Calculated depth profiles of nitrogen (C_{Nsum}, C_{Ntrap} and C_{Ndif}) for three cases: (1) including both processes trapping–detrapping (TD) and stress induce diffusion (SID) (curves 1.1–1.3), (2) only one process SID (curves 2.1–2.3) and (3) including only TD model (curves 3.1–3.3.).

If we exclude the TD process, the penetration depth of nitrogen significantly increases, and surface concentration significantly decreases. This shows that the TD process decreases nitrogen penetration. In the nitrogen depth profile, the characteristic plateau is not well expressed, but it exists. Previously, we were able to get a good fitting result for different experimental results with the SID model without TD [26–31]. The TD model, without SID, gives much less nitrogen penetration depth and higher surface concentration of nitrogen. Curve 3.2 for C_{Ntrap} shows the plateau, but curve 3.3 for C_{Nsum} has no plateau, despite, when SID is included, C_{Nsum} has a plateau (curve 1.3), i.e., by excluding SID, the plateau disappears. It is an important and interesting observation that not only TD but also SID increases the effect of the plateau in the nitrogen depth profile. However, this is not a general rule, and the mentioned effect occurs only at this special case. The plateau in C_{Nsum} curve can be successfully obtained also without SID [17,38,39]. In the case presented in Figure 3, the plateau for C_{Nsum} for TD model is not seen (curve 3.3) because of a big amount of diffusion nitrogen C_{Ndif} (curve 3.1), as $C_{Nsum} = C_{Ntrap} + C_{Ndif}$. If we decrease C_{Ndif}, the plateau would be observed in curve C_{Nsum} [39]. However, considering both models TD and SID, C_{Ndif} cannot be decreased because SID plays only with C_{Ndif} and if we decrease it the influence of SID becomes negligible. From the point of modeling there is a problem, because a good fitting can be obtained in both cases, with and without SID, of course at different parameters, first, at different diffusion coefficients. The true answer would give the direct measurement of partial concentration of nitrogen C_{Ndif}, and C_{Ntrap}, separately; however, experimentally it is not easy to do (or may be impossible). The experimental measurements give results of total nitrogen C_{Nsum} only, which is not very informative to decide working mechanisms and processes. However, many experimental observations confirm the existence of elastic stresses in nitrided austenite, which means that the process of SID also must take place. This means that results presented in Figure 3, i.e., including TD and SID, reflect the processes really taking place during nitriding of ASSs.

That the model TD + SID works properly and shows the good fitting of experimental results at different temperatures. Variation of temperature influences the processes of diffusion and detrapping (both according to Arrhenius law), and influences the level of lattice stresses which decreases with the increase of temperature (see Equations (6) and (7)). Results obtained at 573 K are shown in Figure

4. (in Figure 1 was 643 K). It is seen a good correspondence with experimental results (points) for all crystalline orientations.

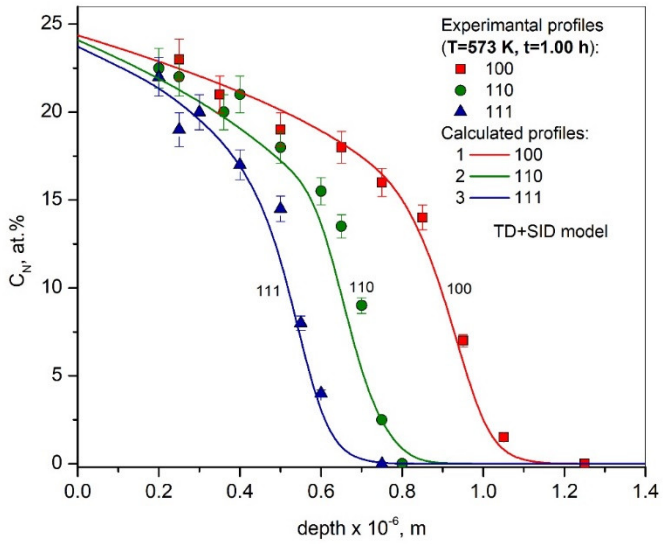

Figure 4. Calculated (lines) and experimental (points) (data from [19]) depth profiles of nitrogen. Nitriding temperature 574 K.

The evolution of nitrogen depth profiles for different lattice orientations are presented in Figure 5. Calculations are performed using values of parameters listed in Table 1, for 573 K temperature of nitriding. It can be seen that with increasing of nitriding time, the profiles for different lattice orientations increasingly differ. The curves for (100) orientation move far away over time from others faster than curves for (110) and curves for (111). The difference between curves 1.1–1.3 after 0.50 h of nitriding is much less compared to the difference between curves 4.1–4.3 after 3.00 h of nitriding. The evolution of surface concentration and penetration depth have the same tendency. Such tendency was also observed experimentally in [53].

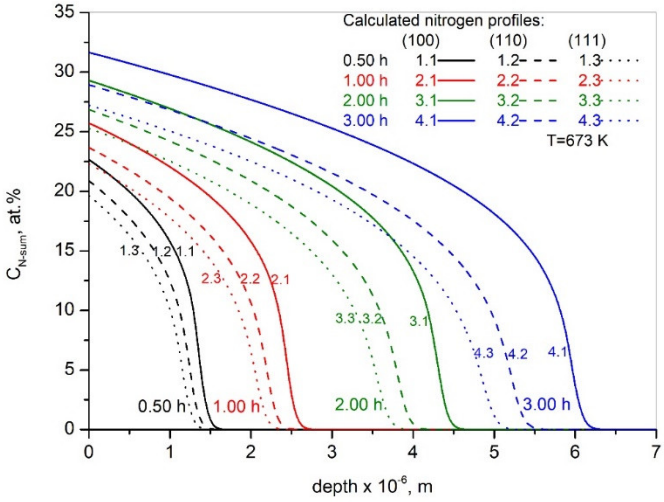

Figure 5. Nitrogen depth profiles evolution in the (100), (110) and (111) oriented single crystals of ASS. Depth profiles after nitriding time 0.50 h, 1.00 h, 2.00 h and 3.00 h at 673 K temperature are presented.

The time dependencies of nitrogen penetration depth from results presented in Figure 5 are plotted in Figure 6, showing the parabolic dependence of penetration depth on time. The penetration depth in this calculations is assumed as distance from the surface till the point with nitrogen concentration 0.3 at.% The curves of penetration depths quite well fit to lines as a functions of $t^{1/2}$ for all lattice orientations.

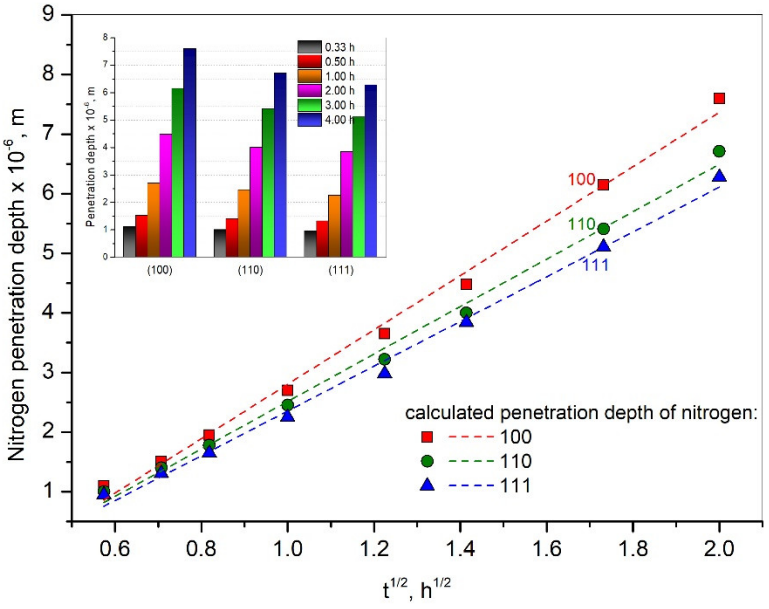

Figure 6. Calculated time dependencies of nitrogen penetrations depth for different crystalline orientations.

The calculated nitrogen penetration depth as a function of diffusion coefficient for three different crystalline orientations (100), (110), and (111) are presented in Figure 7.

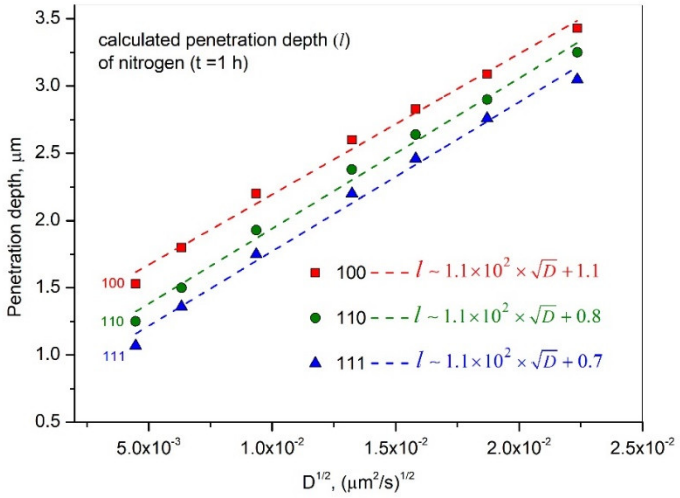

Figure 7. The dependence of penetration depth on diffusion coefficient for different crystalline orientations of AISI 316L single crystals (nitriding duration 1.00 h).

During calculations, the diffusion coefficient was changed by changing temperature according to Arrhenius law. As mentioned before, the diffusion coefficient in our calculations in this work is independent on crystalline orientation. It can be seen from Figure 7 that different penetration of nitrogen for different lattice orientation occurs despite the same diffusion coefficient. With the crystalline orientation only parameters X_{stress} and $\alpha_{N(hkl)}$ are changed. Only these parameters are responsible for different penetration depth of nitrogen for different crystalline orientations despite the same diffusion coefficients. Functions of penetration depth on the square root of diffusion coefficient $D^{1/2}$ show linear dependence, confirming the validity of relation $l \sim \sqrt{Dt}$ for TD + SID model. The small deviations from line functions observed in Figure 7 arise due to some discrepancy to find numerically the points with nitrogen concentration of 0.3 at.%, and some deviations always occur. The lines in Figure 7 are parallel to each other, whereas the slope coefficients of linear equations for all given crystalline orientations presented in the figure coincide. It means that the level of penetration depth anisotropy does not changes with the increase of diffusion coefficient. It is because diffusion coefficient changes with temperature and the increase of temperature decreases the level of lattice stress.

4. Conclusions

Numerical modeling to predict the temporal evolution of the nitrogen concentration depth profile during expanded austenite formation needs the incorporation of coupling between diffusion, trapping, and mechanical stress, as well as by combining both the anisotropy of internal stresses and the anisotropy of adsorption. The anisotropy of lattice stresses and, consequently, the anisotropy of stress-induced diffusion process leads to different nitrogen penetration depth for different crystalline orientations, despite the same diffusion coefficients. The nitrogen penetration depth is highest for the (100) oriented single crystal, smallest for the (111) oriented single crystal, and this difference increases with nitriding time.

Author Contributions: Conceptualization, T.M. and A.G.; methodology, A.G.; software, T.M.; validation, T.M. and A.G; formal analysis, T.M. and A.G; investigation, T.M. and A.G; resources, T.M. and A.G; data curation, T.M. and A.G; writing—original draft preparation, T.M.; writing—review and editing, A.G.; visualization, T.M.; supervision, A.G.; project administration, A.G.; funding acquisition, T.M. and A.G. All authors have read and agreed to the published version of the manuscript.

Funding: This research was funded by RESEACH COUNCIL OF LITHUANIA, grant number MIP-17-103 (Reg. Nr. P-MIP-17-258).

Conflicts of Interest: The authors declare no conflict of interest.

References

1. Menthe, E.; Rie, K.T. Further investigation of the structure and properties of austenitic stainless steel after plasma nitriding. *Surf. Coat. Technol.* **1999**, *116–119*, 199–204, doi:10.1016/S0257-8972(99)00085-7.
2. Menthe, E.; Rie, K.T.; Schultze, J.W.; Simson, S. Structure and properties of plasma-nitrided stainless steel. *Surf. Coat. Technol.* **1995**, *74–75*, 412, doi:10.1016/0257-8972(95)08246-8.
3. Ozturk, O.; Williamson, D.L. Phase and composition depth distribution analyses of low energy, high flux N implanted stainless steel. *J. Appl. Phys.* **1995**, *77*, 3839–3850, doi:10.1063/1.358561.
4. Dahm, K.L.; Dearnley, P.A. On the nature, properties and wear response of s-phase (nitrogen-alloyed stainless steel) coatings on AISI 316L. *Proc. Inst. Mech. Eng. Pt. L J. Mater. Des. Appl.* **2000**, *214*, 181–198, doi:10.1177/146442070021400401.
5. Sun, Y.; Li, X.Y.; Bell, T. X-ray diffraction characterisation of low temperature plasma nitrided austenitic stainless steels. *J. Mater. Sci.* **1999**, *34*, 4793–4802, doi:10.1023/A:1004647423860.
6. Mingolo, N.; Tschiptschin, A.P.; Pinedo, C.E. On the formation of expanded austenite during plasma nitriding of an AISI 316L austenitic stainless steel. *Surf. Coat. Technol.* **2006**, *201*, 4215–4218, doi:10.1177/146442070021400401.
7. Mandl, S.; Rauschenbach, B. Nitrogen diffusion in austenitic stainless steel and the formation of expanded austenite. *Defects Diffus. Metals III* **2001**, 125, doi:10.4028/www.scientific.net/DDF.188-190.125.

8. Wu, D.; Kahn, H.; Dalton, J.C.; Michal, G.M.; Ernst, F.; Heuer, A.H. Orientation dependence of nitrogen supersaturation in austenitic stainless steel during low-temperature gas-phase nitriding. *Acta Mater.* **2014**, *79*, 339, doi:10.1016/j.actamat.2014.07.007.
9. Fewell, M.P.; Mitchell, D.R.G.; Priest, J.M.; Short, K.T.; Collins, G.A. The nature of expanded austenite. *Surf. Coat. Technol*. **2000**, *131*, 300–306, doi:10.1016/S0257-8972(00)00804-5.
10. Keddam, M.; Marcos, G.; Thiriet, T.; Czerwiec, T.; Michel, H. Microstructural characterization of the expanded austenite formed on the plasma nitrided AISI 316 L steel. *Mater. Tech.* **2013**, *101*, 204, doi:10.1051/mattech/2013064.
11. Somers, M.A.J.; Kücükyildiz, Ö.C.; Ormstrup, C.A.; Alimadadi, H.; Hattel, J.H.; Christiansen, T.L.; Winther, G. Residual stress in expanded austenite on stainless steel; origin, measurement, and prediction. *Mater. Perform. Charact.* **2018**, *7*, 693–716, doi:10.1520/MPC2017014511.
12. Christiansen, T.L.; Hummelshøj, T.S.; Somers, M.A.J. Expanded austenite, crystallography and residual stress. *Surf. Eng.* **2010**, *26*, 242–247, doi:10.1179/026708410x12506870724316.
13. Riviere, J.P.; Pichon, L.; Drouet, M.; Poquillon, D.; Galdikas, A. Silicon based coatings deposited by dynamic ion mixing for oxidation protection of a Ti6242 alloy. *Surf. Coat. Technol.* **2007**, *201*, 8343–8347, doi:10.1016/j.surfcoat.2006.01.083.
14. Picard, S.; Memet, J.B.; Sabot, R.; Grosseau-Poussard, J.L.; Rivière, J.P.; Meilland, R. Corrosion behaviour, microhardness and surface characterisation of low energy, high current ion implanted austenitic stainless steel. *Mater. Sci. Eng. A* **2001**, *303*, 163–172, doi:10.1016/s0921-5093(00)01841-4.
15. Stinville, J.C.; Villechaise, P.; Templie, C.; Riviere, J.P.; Drouet, M. Lattice rotation induced by plasma nitriding in a 316L polycrystalline stainless steel. *Acta Mater*. **2010**, *58*, 2814–2821, doi:10.1016/j.actamat.2010.01.002.
16. Borgioli, F. From austenitic stainless steel to expanded austenite-S phase: Formation, characteristics and properties of an elusive metastable phase. *Metals* **2020**, *10*, 187, doi:10.3390/met10020187.
17. Martinavičius, A.; Abrasonis, G.; Möller, W. Influence of crystal orientation and ion bombardment on the nitrogen diffusivity in single-crystalline austenitic stainless steel. *J. Appl. Phys.* **2011**, *110*, 075907, doi:10.1063/1.3646493.
18. Akhlaghi, M.; Jung, M.; Meka, S.R.; Fonović, M.; Leineweber, A.; Mittemeijer, E.J. Dependence of the nitriding rate of ferritic and austenitic substrates on the lattice orientation of surface grains; gaseous nitriding of Fe-Cr and Ni-Ti alloys. *Philos. Mag.* **2015**, *95*, 4143–4160, doi:10.1080/14786435.2015.1115906.
19. Menéndez, E.; Templier, C.; Garcia-Ramirez, P.; Santiso, J.; Vantomme, A.; Temst, K.; Nogués, J. Magnetic properties of single crystalline expanded austenite obtained by plasma nitriding of austenitic stainless steel single crystals. *ACS Appl. Mater. Interfaces* **2013**, *5*, 10118–10126, doi:10.1021/am402773w.
20. Fewell, M.P.; Priest, J.M. High-order diffractometry of expanded austenite using synchrotron radiation. *Surf. Coat. Technol.* **2008**, *202*, 802–1815, doi:10.1016/j.surfcoat.2007.07.062.
21. He, H.; Zou, J.X.; Dong, C.; Czerwiec, T.; Michel, H. Stress induced anisotropic diffusion during plasma-assisted nitriding of a Ni-based alloy. *Mater. Sci. Forum.* **2005**, *475–479*, 3669–3672, doi:10.4028/www.scientific.net/msf.475-479.3669.
22. Kahn, H.; Michal, G.M.; Ernst, F.; Heuer, A.H. Poisson effects on X-ray diffraction patterns in low-temperature-carburized austenitic stainless steel. *Metall. Mater. Trans. A* **2009**, *40A*, 1799–1804, doi:10.1007/s11661-009-9814-4.
23. Mändl, S.; Rauschenbach, B. Anisotropic strain in nitrided austenitic stainless steel. *J. Appl. Phys.* **2000**, *88*, 3323–3329, doi:10.1063/1.1289520.
24. Jespersen, F.N.; Hattel, J.H.; Somers, M.A.J. Modelling the evolution of composition-and stress-depth profiles in austenitic stainless steels during low-temperature nitriding. *Model. Simul. Mat. Sci. Eng*. **2016**, *24*, 025003, doi:10.1088/0965-0393/24/2/025003.
25. Kücükyildiz, Ö.C.; Sonne, M.R.; Thorborg, J.; Somers, M.A.J.; Hattel, J.H. Thermo-chemical-mechanical simulation of low temperature nitriding of austenitic stainless steel; inverse modelling of surface reaction rates. *Surf. Coat. Technol.* **2020**, *381*, 125145, doi:10.1016/j.surfcoat.2019.125145.
26. Moskalioviene, T.; Galdikas, A. Stress induced nitrogen diffusion in nitrided austenitic stainless steel. *Mater. Sci. Medz.* **2011**, *17*, 11–15, doi:10.5755/j01.ms.17.1.241.
27. Galdikas, A.; Moskalioviene, T. Swelling effect on stress induced and concentration dependent diffusion of nitrogen in plasma nitrided austenitic stainless steel. *Comput. Mater. Sci.* **2013**, *72*, 140–145, doi:10.1016/j.commatsci.2013.02.007.

28. Moskalioviene, T.; Galdikas, A. The effect of hydrogen on plasma nitriding of austenitic stainless steel: Kinetic modeling. *Metall. Mater. Trans. A* **2015**, *46*, 5588–5595, doi:10.1007/s11661-015-3183-y.
29. Moskalioviene, T.; Galdikas, A. Kinetic model of anisotropic stress assisted diffusion of nitrogen in nitrided austenitic stainless steel. *Surf. Coat. Technol.* **2019**, *366*, 277–285, doi:10.1016/j.surfcoat.2019.03.054.
30. Galdikas, A.; Moskalioviene, T. Stress induced nitrogen diffusion during nitriding of austenitic stainless steel. *Comput. Mater. Sci.* **2010**, *50*, 796–799, doi:10.1016/j.commatsci.2010.10.018.
31. Moskalioviene, T.; Galdikas, A. Lattice orientation dependence of nitrogen mass transport in austenitic stainless steel. *Metals* **2020**, *10*, 615, doi:10.3390/met10050615.
32. Zangwill, A. *Physics at Surfaces*; Cambridge University Press: New York, NY, USA, 1988.
33. Czerwiec, T.; Andrieux, A.; Marcos, G.; Michel, H.; Bauer, P. Is "expanded austenite" really a solid solution? Mossbauer observation of an annealed AISI 316L nitrided sample. *J. Alloys Compd.* **2019**, *811*, 151972, doi:10.1016/j.jallcom.2019.151972.
34. Oddershede, J.; Christiansen, T.L.; Stahl, K.; Somers, M.A.J. Extended X-ray absorption fine structure investigation of nitrogen stabilized expanded austenite. *Scr. Mater.* **2010**, *62*, 290–293. doi:10.1016/j.scriptamat.2009.11.021
35. Tao, X.; Matthews, A.; Leyland, A. On the Nitrogen-Induced Lattice Expansion of a Non-stainless Austenitic Steel, Invar 36®, Under Triode Plasma Nitriding. *Metall. Mater. Trans. A* **2020**, *51*, 436–447, doi:10.1007/s11661-019-05526-0.
36. Parascandola, S.; Moller, W.; Williamson, D.L. The nitrogen transport in austenitic stainless steel at moderate temperatures. *Appl. Phys. Lett.* **2000**, *76*, 2194–2196, doi:10.1063/1.126294.
37. Riviere, J.P.; Cahoreau, M.; Meheust, P. Chemical bonding of nitrogen in low energy high flux implanted austenitic stainless steel. *J. Appl. Phys.* **2002**, *91*, 6361, doi:10.1063/1.1469691.
38. Martinavicius, A.; Abrasonis, G.; Möller, W.; Templier, C.; Rivière, J.P.; Declémy, A.; Chumlyakov, Y. Anisotropic ion-enhanced diffusion during ion nitriding of single crystalline austenitic stainless steel. *J. Appl. Phys.* **2009**, *105*, 093502, doi:10.1063/1.3120912.
39. Moskalioviene, T.; Galdikas, A.; Riviere, J.P.; Pichon, L. Modeling of nitrogen penetration in polycrystalline AISI 316L austenitic stainless steel during plasma nitriding. *Surf. Coat. Technol.* **2011**, *205*, 3301–3306, doi:10.1016/j.surfcoat.2010.11.060.
40. Mändl, S.; Scholze, F.; Neumann, H.; Rauschenbach, B. Nitrogen diffusivity in expanded austenite. *Surf. Coat. Technol.* **2003**, *174–175*, 1191–1195, doi:10.1016/S0257-8972(03)00454-7.
41. Gu, X.; Michal, G.M.; Ernst, F.; Kahn, H.; Heuer, A.H. Numerical Simulations of Carbon and Nitrogen Composition-Depth Profiles in Nitrocarburized Austenitic Stainless Steels. *Metall. Mater. Trans. A* **2014**, *45*, 4268–4279, doi:10.1007/s11661-014-2377-z.
42. Christiansen, T.; Dahl, K.V.; Somers, M.A.J. Nitrogen diffusion and nitrogen depth profiles in expanded austenite: Experimental assessment, numerical simulation and role of stress. *Mater. Sci. Technol.* **2008**, *24*, 159–167, doi:10.1179/026708307x232901.
43. Fischer, F.D.; Svoboda, J.; Kozeschnik, E. Interstitial diffusion in systems with multiple sorts of traps. *Model Simul. Mat. Sci. Eng.* **2013**, *21*, 025008, doi:10.1088/0965-0393/21/2/025008.
44. Svoboda, J.; Fischer, F.D.; Fratzl, P. Diffusion and creep in multi-component alloys with non-ideal sources and sinks for vacancies. *Acta Mater.* **2006**, *54*, 3043–3053, doi:10.1016/j.actamat.2006.02.041.
45. Svoboda, J.; Fischer, F.D. Modelling for hydrogen diffusion in metals with traps revisited. *Acta Mater.* **2012**, *60*, 1211–1220, doi:10.1016/j.actamat.2011.11.025.
46. Möller, W.; Parascandola, S.; Telbizova, T.; Günzel, R.; Richter, E. Surface processes and diffusion mechanisms of ion nitriding of stainless steel and aluminium. *Surf. Coat. Technol.* **2001**, *136*, 73–79, doi:10.1016/s0257-8972(00)01015-x.
47. Oriani, R. The diffusion and trapping of hydrogen in steel. *Acta Metall.* **1970**, *18*, 147–157, doi:10.1016/0001-6160(70)90078-7.
48. Sofronis, P.; McMeeking, R.M. Numerical analysis of hydrogen transport near a blunting crack tip. *J. Mech. Phys. Solids* **1989**, *37*, 317–350, doi:10.1016/0022-5096(89)90002-1.
49. Krom, A.H.M.; Koers, R.W.J.; Bakker, A. Hydrogen transport near a blunting crack tip. *J. Mech. Phys. Solids* **1999**, *47*, 971–992, doi:10.1016/s0022-5096(98)00064-7.
50. Zhang, L.; Barrett, R.; Cloetens, P.; Detlefs, C.; Rio, M.S. Anisotropic elasticity of silicon and its application to the modelling of X-ray optics. *J. Synchrotron Radiat.* **2014**, *21*, 507–517, doi:10.1107/S1600577514004962.

51. He, H.; Czerwiec, T.; Dong, C.; Michel, H. Effect of grain orientation on the nitriding rate of a nickel base alloy studied by electron backscatter diffraction. *Surf. Coat. Technol.* **2003**, *163–164*, 331–338, doi:10.1016/S0257-8972(02)00611-4.
52. Zener, C. Contributions to the Theory of Beta-Phase Alloys. *Phys. Rev*. **1947**, *71*, 846–851, doi:10.1103/physrev.71.846.
53. Templier, C.; Stinville, J.C.; Villechaise, P.; Renault, P.O.; Abrasonis, G.; Riviere, J.P.; Martinavicius, A.; Drouet, M. On lattice plane rotation and crystallographic structure of the expanded austenite in plasma nitrided AISI 316L steel. *Surf. Coat. Technol.* **2010**, *204*, 2551–2558, doi:10.1016/j.surfcoat.2010.01.041.
54. Juul, N.Y.; Oddershede, J.; Beaudoin, A.; Chatterjee, K.; Koker, M.K.A.; Dale, D.; Shade, P.; Winther, G. Measured resolved shear stresses and Bishop-Hill stress states in individual grains of austenitic stainless steel. *Acta Mater.* **2017**, *141*, 388–404, doi:10.1016/j.actamat.2017.09.021.
55. Gressmann, T.; Wohlschlogel, M.; Shang, S.; Welzel, U.; Leineweber, A.; Mittemeijer, E.J.; Liu, Z.K. Elastic anisotropy of γ′-Fe4N and elastic grain interaction in γ′-Fe4N1−y layers on α-Fe: First-principles calculations and diffraction stress measurements. *Acta Mater.* **2007**, *55*, 5833–5843. 10.1016/j.actamat.2007.07.001.